Bayesian compressive sensing for recovering the time-frequency representation of under-sampled lamb wave signals

Zhe Wang[a], Shen Wang[a], Qing Wang[b], Zaifu Zhan[a], Wei Zhao[a], Songling Huang[a*]

[a]State Key Laboratory of Power System, Department of Electrical Engineering, Tsinghua University, Beijing 100084, China
[b]Department of Engineering, Durham University, Durham, UK

Corresponding author: Songling Huang (email: huangsling@tsinghua.edu.cn)

This research was financially supported by the National Key Research and Development Program of China (Grant No. 2018YFF01012802), National Natural Science Foundation of China (NSFC) (Grant No. 52077110, 51677093 and 51777100).

ABSTRACT The characteristic extraction of ultrasonic Lamb wave is the prerequisite for its efficient utilization in the structural health monitoring. In the situation of intentional signal compression or unexpected data missing, the accurate recovery of contained information is challenging. To address this problem, this work proposes the time-frequency representation (TFR) reconstruction scheme for undersampled Lamb wave signal. Unlike the conventional method, both the sparse prior and structural sparse prior in the two dimensional plane are considered in the design of Bayesian compressive sensing. The simulated signal is adopted to validate the effectiveness of the proposed method. Furthermore, different ratios of available samples are investigated to analyze the recovery ratio of TFR. Even if the available samples are smaller than those from the Nyquist rate, the TFR recovery ratio can reach 70%. The experiments using array transducers in noisy environments are also conducted. The time-of-flight information extracted from the recovered TFR is accurate and the relative error is smaller than 3%. Besides, the comparisons with conventional schemes for compressive sensing are carried out to demonstrate its superiority.

INDEX TERMS Bayesian inference, Compressive sensing, Sparse prior, Time-frequency representation, Time-of-flight

1.Introduction

Lamb wave is the commonly used guided wave in the structural health monitoring of plates [1–5]. After propagating through the structure, the wave can be received to extract the encoded information and further locate, even image the damage [6–9]. Lamb wave owns the natures of dispersion and multi-modes and they bring the challenges for its effective utilization [10–12]. Therefore, the appropriate signal post-processing method is pivotal in the interpretation of Lamb wave.

The received Lamb wave signal is typically non-stationary signal. Corresponding signal processing techniques have been developed to accomplish the Lamb wave exploitation [13–15]. The guided wave field was described by a wavenumber analysis method and the frequency-wavenumber spectra was applied to identify the structural discontinuity [16]. The theoretical basis signal was calculated and the correlation analysis between basis signal and received signal was conducted to implement the mode separation [17]. The singular value decomposition approach had been introduced to analyze the array signal and obtain the timeof- flight (TOF) of scattered wave [18]. Besides, the time-frequency representation (TFR) provides an efficient method. The cross Wigner-Ville distribution (xWVD) was employed on the received signal and excitation signal to separate the Lamb wave modes in the time-frequency plane [19]. The wavelet network was proposed to extract the damage features from the signal and further estimate the damage location and severity [20]. The warped frequency transform, chirplet transform, S transform, and the like had also been investigated to analyze the disperse Lamb wave [21–24]. These methods proved to be available in different aspects, however, they ignored the data compression or data missing problem in the long-term and large-area inspection.

For Lamb wave imaging, usually dense acoustic rays need to cover the whole plate structure. The huge amounts of inspection data lead to the storage and transmission problem [25]. Compressive sensing attracted considerable attention due to its different perspective compared with Shannon's theorem [26–28]. The compressed sampling provides a potential way to decrease the data amount. In addition, the removal of impulsive noise may cause the missing of samples [29]. Therefore, a suitable post-processing scheme is required to deal with the incomplete signal [30]. The structural responses were compressed with different compression ratios by the random measurement and the recovery process was solved through the convex optimization [31]. The dictionary algorithm had been designed to recover the Lamb wave through the sparse spatial domain [32]. Combining the probability and statistics theory, Bayesian compressive sensing and improved strategy for cluster sparse signals had been developed [33,34]. The TFR can present the Lamb wave effectively in the two-dimensional plane, and further the time-relevant or frequency-relevant or time-frequency relevant characteristics can be obtained. However, to the best of the authors' knowledge, the TFR had not been directly recovered from the incomplete Lamb wave signal.

In this work, the Bayesian compressive sensing with structural sparse prior has been proposed to extract the time-frequency characteristics of the undersampled Lamb wave. The Lamb wave signal is undersampled in a random way and only a certain proportion of samples are available. The relation of TFR and instantaneous autocorrelation function (IAF) is applied to construct the compressive sensing model. Then the sparsity and structural sparsity of time-frequency distribution are both utilized to reconstruct the TFR. The maximum energy time-frequency ridge is obtained from the TFR and further the TOF can be extracted for the Lamb wave tomography. The successful recovery ratios of the TFR grids are also investigated in different undersampled situations. The proposed method is also compared with conventional compressive sensing and Bayesian compressive sensing. In the basis of compressive sensing, the proposed method introduces the Bayesian inference. The combining of sparse prior and structural sparse prior can explore deeper feature of dispersive Lamb wave. It helps to exert the superiority of compressive sensing and make the proposed method achieve the highest recovery ratios. Besides, the extracted TOFs are compared with those from threshold method and cross correlation method to verify the accuracy in the TFR recovery.

The remainder of this paper is organized as follows. Section II outlines the detailed scheme for the TFR reconstruction from the undersampled Lamb wave signal. In section III, the validation using the simulated signal is conducted to demonstrate the effectiveness of proposed method. Experimental investigations and further comparisons with conventional compressive sensing are presented in section IV. Concluding remarks are summarized in section V.

2. Time-frequency characteristics extraction scheme

The overall diagram of the proposed scheme is depicted in Fig. 1. The incomplete Lamb wave signal is recovered in the time-frequency domain using sparse prior and structural sparse prior. The sparse prior means that most of the entries in the TFR are zero values. Due to the features of wavepackets in structural sparse prior is also considered in the proposed scheme. The TFR can facilitate the signal analysis and characteristics recognition efficiently. In this context, the TOF is extracted for further utilization. The detailed procedures are given in the following sections.

2.1 *Framework of compressive sensing*

If the signal **x** only owns limited non-zero elements, the ‘‘sensing” of original signal can be accomplished using a measurement matrix $\Phi \epsilon R^{MxN}$. This process can be described as follows [35]:

$$\mathbf{y} = \Phi\mathbf{x}. \tag{1}$$

Where **y** is the observed value. Usually, $M \ll N$ and then y has smaller data dimensions than **x**.

The precondition of the compressive sensing is that the signal is sparse or at least it is sparse in a certain domain. The ‘‘sparse” means that the number of non-zero entries is limited. In the case of guided wave signal, it is not sparse in the time domain mathematically. Therefore, it must be transformed to the other domain and it can be expressed as:

$$\mathbf{s} = \Psi\prime\mathbf{x}. \tag{2}$$

where $\Psi,$ is the transformation matrix.

The calculated coefficient **s** after the proper transformation can be sparse. Combining (1) and (2), the compressive sensing model can be obtained:

$$\mathbf{y} = \Phi\Psi\mathbf{s} = \Theta\mathbf{s}. \tag{3}$$

To recover the original signal x from the observed data, the measurement matrix Φ needs to satisfy the restricted isometry property (RIP). Because the dimensions of observed values **y** are smaller than that of original signal **x**, the conventional method can not accomplish the inverse recovery of the signal. Compressive sensing has attracted considerable attention recently and Bayesian compressive sensing is the new model which will be analyzed and adapted to the Lamb wave signal.

2.2 *Bayesian compressive sensing for TFR*

The aim of Bayesian compressive sensing in this work I sto recover the time-frequency signatures from the undersampled signal. The original signal is denoted as x(t) and the undersampled data is denoted as y(n). The signal can be correlated with its time-frequency distribution by using the instantaneous autocorrelation function (IAF) [36]. The relation of classical Wigner-Ville distribution (WVD) and IAF constitutes the basis of compressive sensing model. The IAF can be expressed as:

$$R(n,\tau) = y(n+\tau)y^{*}(n-\tau) \tag{4}$$

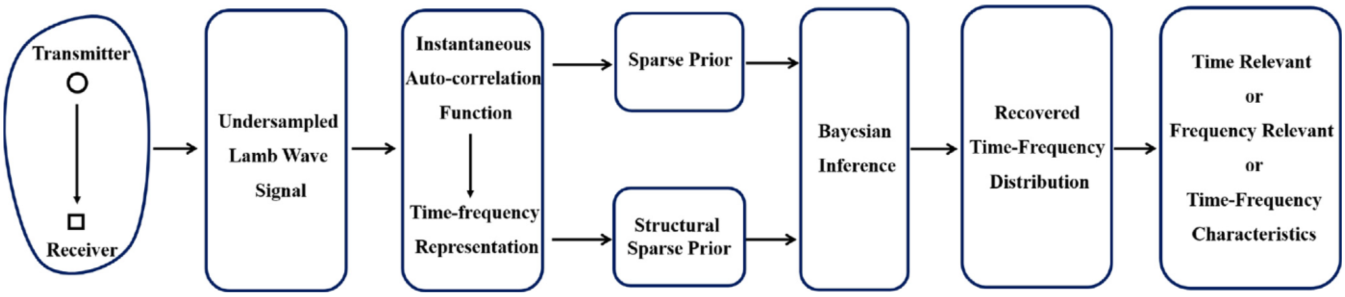

Fig.1. The block diagram for the time-frequency characteristics extraction scheme through the structural sparse Bayesian compressive sensing.

where n is the discrete time point and s denotes the time-lag. Considering putting all the R from different time-lags and time points together, the IAF matrix **R** can be obtained. The WVD can be calculated by the discrete Fourier transform of IAF with respect to timelag:

$$\mathbf{W}(n,f) = \mathscr{F}_{\tau}[\mathbf{R}(n,\tau)] \tag{5}$$

Where $\mathscr{F}\tau$ represents the discrete Fourier transform. The WVD owns accurate time-frequency analysis capability for one single signal. However, the cross-term will be generated when the signal is the summation of multiple signals or the signal has multiple concentrated areas in the TFR. The time-frequency kernel, which is considered as the window function for WVD, can be applied to filter this interference. Then, the general form or Cohen's class of TFR is obtained:

$$\mathbf{C}(n,f) = \mathscr{F}_{\tau}[\mathbf{R}\prime(n,\tau)] \tag{6}$$

Where $\mathbf{R}\prime$ is the matrix of general IAF and **c** denotes the Cohen's class. The general IAF can be expressed as:

$$R\prime(n,\tau) = \frac{1}{2\pi}\sum_{u} R(u,\tau)g(n-u,\tau) \tag{7}$$

where g is the smoothing kernel and R' is the general IAF. Different kernels will determine different time-frequency distributions. For the inverse process of (6), it can be given by:

$$\mathbf{R}(\tau,n) = \mathscr{F}_f^{-1}\mathbf{C}(f,n) + \mathbf{W} \tag{8}$$

where **W** is the error which is considered as the Gaussian white noise with mean of zero and covariance matrix of $\sigma^2\mathbf{I}$.

It is worth noting that each column of the matrix conforms to the compressive sensing model of (3):

$$\mathbf{r} = \Theta\mathbf{c} + \mathbf{w} \tag{9}$$

where Θ is the notation for $\mathscr{F}_f^{-1}$.

The **c** in the time-frequency domain is sparse and conventionally, the sparse Bayesian learning assumes that each entry of c satisfies the Gaussian distribution with variance of γ[33]:

$$p(c_i;\gamma_i) = \mathcal{N}(0,\gamma_i^{-1}) \tag{10}$$

where p is the probability density, N denotes the Gaussian distribution and ci is the unknown parameter which will be estimated by the algorithm. The ci is called the hyperparameter and it obeys the Gamma distribution:

$$p(\gamma;a,b) = \prod_i \Gamma(\gamma_i;a,b) \tag{11}$$

where a and b are the two parameters in the Gamma distribution.

The illustration of Bayesian compressive sensing model is shown in Fig. 2. The hyperparameters control the process of TFR recovery. Due to the sparse prior, usually most of the γ_i will become zero, thus, the corresponding c_i will be zero. In this model, the hyperparameters of γ_i are independent with each other and the structural information is not utilized sufficiently.

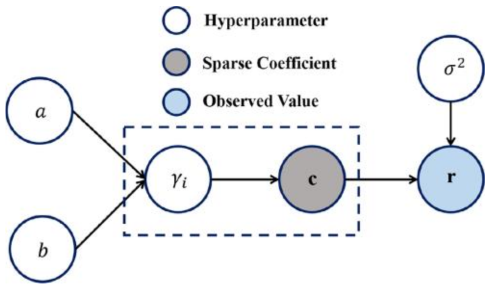

Fig.2. The illustration of Bayesian compressive sensing model.

2.3 Structural Sparse prior design

Since the excitation signal of Lamb wave owns certain patterns in the time-frequency distribution, the received signal also presents prior properties in the two-dimensional plane of TFR. Specifically, the time-frequency domain forms the block sparse structure and each entry is influenced by adjacent elements. The coupled model is expressed as:

$$p(\mathbf{C};\alpha) = \prod_l\prod_m \mathcal{N}(c_{l,m};0,\alpha_{l,m}^{-1}) \tag{12}$$

where $\alpha_{l,m}$is defined as:

$$\alpha_{l,m} \triangleq \gamma_{l,m} + \xi \sum_{(i,j)\in N(l,m)} \gamma_{ij} \tag{13}$$

where N(l,m) is the adjacent grid of (l,m) and ξ is the coupling coefficient. The TFR can be regarded as a two-dimensional picture composed of discrete grids. The horizontal axis is the time and the vertical axis is the frequency. The grid in the time scale is depended on the time interval of the discrete signal. The grid in the frequency scale is also derived from the sampling rate divided by number of sampling points.

Due to the dispersion of Lamb wave, the waves of different frequencies propagate in different velocities. In this context, the excitation signal of Lamb wave is a windowed sinusoidal signal which owns a narrow bandwidth. After propagating a certain distance, the time-frequency ridge of Lamb wave will be in an oblique line according to the dispersion. Considering the TFR of disperse Lamb wave, the N(l.m) is defined as:

$$N(l,m) \triangleq \{(l-1,m-1),(l-1,m+1),\\ (l+1,m-1),(l+1,m+1)\} \tag{14}$$

Similarly, the hyperpriors of hyperparameters are Gamma distributions:

$$p(\gamma) = \prod_l\prod_m \Gamma(\gamma_{l,m};a,b)$$

The illustration of this model with structural sparse prior is shown in Fig. 3. When the grid (l,m) is in the margin of the time-frequency plane, the set of $\alpha_{l,m}$ will also be modified. The parameter ξ which belongs to the range of 0~1 indicates the degree of the coupling from surrounding elements. When this coefficient is equal to zero, this model is degraded into the conventional Bayesian compressive sensing.

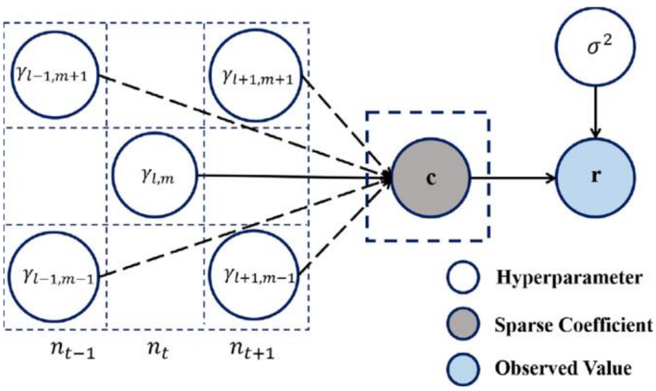

Fig.3. The Bayesian compressive model with structural sparse prior in two-dimensional situation.

2.4 Bayesian inference

To make it clear in the following description, the noise variance σ^2 is denoted as Λ. According to the Bayesian formula, the posterior distribution of **c** is expressed as [37]:

$$p(\mathbf{c};\gamma,\mathbf{r},\Lambda) \propto p(\mathbf{r};\mathbf{c},\Lambda)p(\mathbf{c};\gamma) \tag{16}$$

Where p(**r**;**c**;Λ) is the conditional probability density function of **r**:

$$p(\mathbf{r};\mathbf{c},\Lambda) = \frac{1}{(\sqrt{2\pi\Lambda})^N}\exp(-\frac{1}{2\Lambda}\|\mathbf{r}-\Theta\mathbf{c}\|^2) \tag{17}$$

where N is the dimension of **r**. To learn from the noise situation, the Gamma hyperprior is assigned to Λ:

$$p(\Lambda) = \Gamma(\Lambda;c,d) \tag{18}$$

where a and b are the two parameters in the Gamma distribution.

This posterior of c on the whole also complies with the Gaussian distribution. Then its mean and covariance matrix can be obtained from the following equations:

$$\mu = \Lambda\Sigma\Theta^T\mathbf{r} \tag{19}$$

$$\Sigma = (\Lambda\Theta^T\Theta + \mathbf{D})^{-1} \tag{20}$$

Where μ and Σ are the mean and covariance matrix, respectively. **D** is the diagonal matrix and is defined as:

$$\mathbf{D} \triangleq \mathrm{diag}[\alpha_{1,1},\cdots,\alpha_{L,M}] \tag{21}$$

The object of Bayesian inference is to obtain the maximum a posterior (MAP) of the time-frequency distribution. The expectation–maximization (EM) approach can be employed to learn the sparse property. This approach is divided into two steps with an iterative process. In the first E-step, given the estimated hyperparameters, calculate the posterior distribution of **c** based on (16). In the second M-step, through maximizing the bound of posterior probability p $(\gamma, \mathrm{A}; \boldsymbol{r})$ which is called the Q-function, the hyperparameters of γ, A can be calculated. The generalized approximate message passing (GAMP) algorithm provides a computationally efficient method. The literature [38,39] gives the detailed description. The diagram of this EM process is summarized in Fig. 4. The iteration will be terminated when the difference between two estimations are within a limited error ε.

3. Test with simulated lamb wave

The generation of Lamb wave is conducted in the finite element software COMSOL Multiphysics. The geometric model of plate is constructed and the force is loaded on the left boundary to simulate the excitation of Lamb wave. The force is in the form of a tone-burst pulse and its equation is given by:

$$P(t) = (0.54 - 0.46\cdot\cos(2\pi t/T))\cdot\sin(2\pi ft) \tag{22}$$

where T is the time duration of pulse and f is the center frequency. The corresponding parameters of plate and pulse are given in Table 1.

The plate model and the pulse are depicted in Fig. 5. The Lamb wave receiver point is set at a distance of 2000 mm away from the excitation boundary. The original sampling rate for the signal is 1 MHz. To simulate the undersampled situation, 40% of the original samples are considered as the missing points and set as zero values on their positions. The positions of missing points are random and they are marked as small red circles in Fig. 6. Thus, the available samples are equal to 60% of the total samples. It can be seen that two main wave-packets appear in the signal. They are the two modes of Lamb wave since the generated modes are not controlled. According to the dispersion relation of Lamb wave, the group velocities of S_0 mode and A_0 mode are 5279 and 3127 m/s, respectively. Therefore, the first wave-packet is symmetric S_0 mode which owns the faster velocity. The second wave-packet is the anti-symmetric A_0 mode.

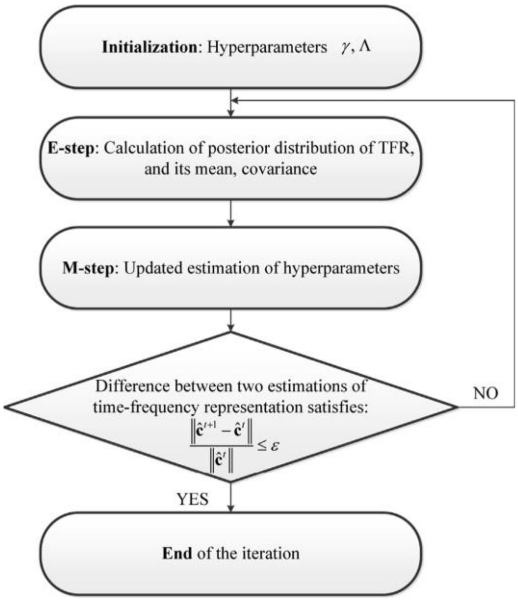

Fig.4. The expectation-maximization approach in an iterative process is applied to solve the sensing problem.

Table 1
Parameters of the plate and pulse for Lamb wave generation.

Plate Thickness	Corresponding Symbol	Value
Plate Thickness	h	4mm
Plate Young's Modulus	E	205 GPa
Plate Density	ρ	7850kg$\cdot m^{-3}$
Plate Poisson's Ratio	v	0.28
Pulse Frequency	f	200 kHz
Paulse Amplitude	A	1
Paulse Time Duration	30	μs

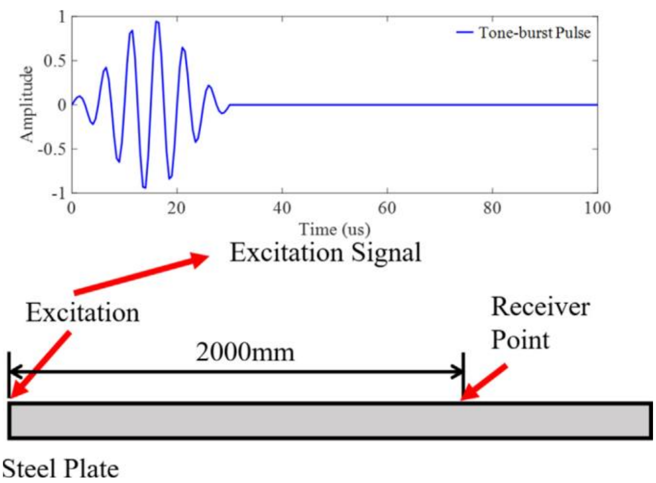

Fig. 5. The geometric model of plate is built and the paulse is located to generate the simulated Lamb wave.

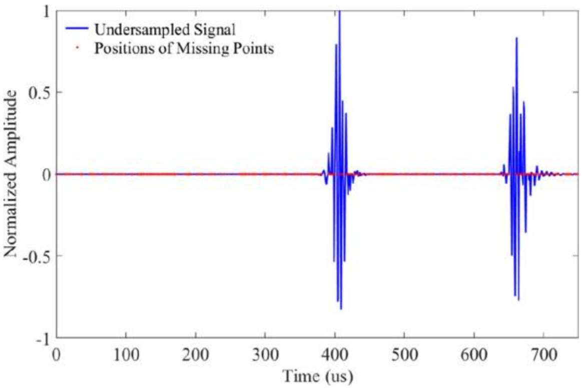

Fig.6. The undersampled waveform in the simulated Lamb wave signal. The red circles indicate the positions of missing points.

In the initialization process, the parameters of γ, Λ are set as 0. The hyperparameters in the Gamma distribution are set as follows: a = 1.5, b=10^{-6}, c = 1, and d=10^{-6}. The coupling coefficient ξ is set as 0.3. The error for the termination of the iteration is set as 0.03.

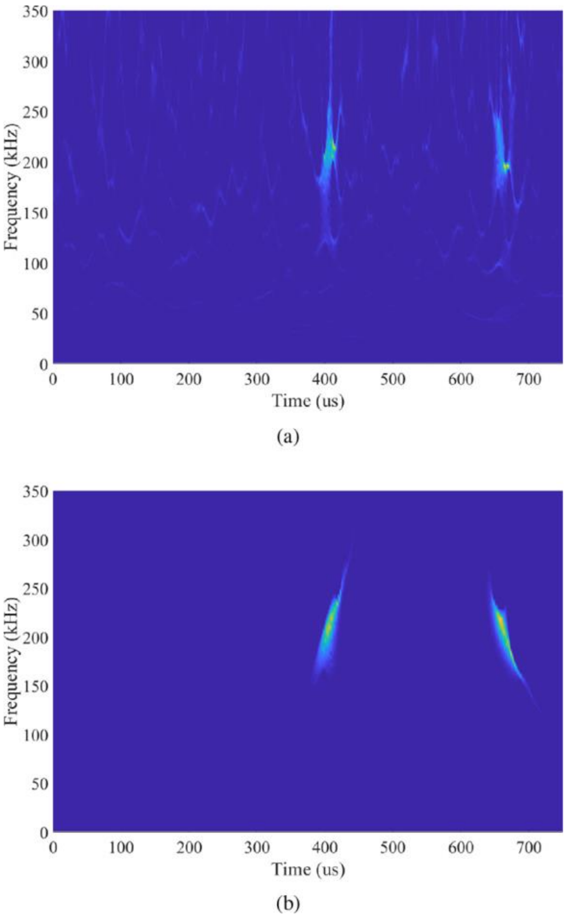

Fig.7. The obtained time-frequency distribution. (a) Results of direct transformation using the undersampled signal. (b) Results of the proposed structural sparse Bayesian compressive sensing.

The undersampled signal is firstly directly transformed to the time-frequency distribution. The results are shown in Fig. 7a. The two wave-packets form two concentrated areas in the TFR, however, the disturbances with non-negligible values are spread over the whole two-dimensional plane. This is not only caused by cross-terms, but also by the missing points. They react together to bring the disturbances. These disturbances will negatively influence the recognition of time-frequency relevant characteristics, which is adverse to the accurate information extraction. After implementing the proposed structural sparse Bayesian compressive sensing, the obtained time-frequency distribution from the undersampled signal is shown in Fig. 7b. It can be observed that most of the time-frequency regions are zero and conform to the sparse property. Meanwhile, the TFR presents the group sparse characteristic, which means only several concentrated areas have the important values. The time-frequency distributions of the two wave-packets also show in the oblique shape in the plane, which is coincident with the theoretical analysis. Due to the different dispersion relationship, the TFRs of A_0 mode and S_0 mode present different oblique patterns. The direct TFR of original simulated signal without undersampling is shown in Fig. 8. The time frequency aggregation in the TFR accords with the Lamb wave characteristics. The structure aware Bayesian compressive sensing help to recover the TFR in a high accuracy.

The time information corresponding to the center frequency 200 kHz can be readily obtained from the time-frequency ridge. In detail, the times of the S_0 mode and A_0 mode are 405 and 667 μs, respectively. Considering the center time of the pulse is 15 μs, the TOFs of S_0 mode and A_0 mode are 390 and 652 μs, respectively. Combining the group velocities of these two modes, the theoretical TOFs are 398 and 655 μs, respectively. The relative error of obtained TOFs compared with the theoretical values are both smaller than 2%. Therefore, the calculated TOFs are rather accurate. The proposed approach allows the direct information extraction from the compressed signal. The TOF is the key parameter to input in the tomography algorithm, which will be conducted in the experimental part.

To further study the success rate of the Bayesian compressive sensing, the reconstruction of TFR is employed under different cases of available samples. The available ratios of samples vary from 5% to 75%, then the obtained grids in the TFR are compared with the recovered TFR grids from full samples. Since the small values might exist in some grids of TFR and it is meaningless to consider these grids, the threshold is set to count on the large values in the TFR. Then the recovered grids with values larger than the threshold are counted and used to calculate the recovery ratio. The threshold is set as 5% of the maximum amplitude in the TFR.

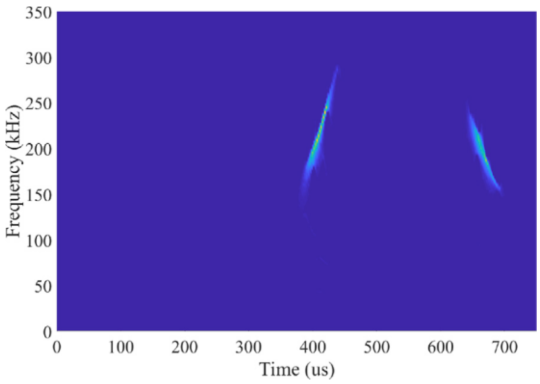

Fig.8. The direct TFR of original simulated signal without undersampling.

All grids in the TFR are searched and the number is recorded. The recovery ratio is expressed as:

$$RR = \frac{N_{rec}}{N_{full}} \quad (23)$$

where N_{rec} and N_{all} denotes the numbers of grids in the TFR from proposed method and that from the full samples, respectively. It needs to note that the grids with values larger than the threshold are counted.

The proposed method is compared with conventional compressive sensing and the Bayesian compressive sensing. The results of available samples and the recovered TFR grid ratios are shown in Fig. 9. It can be seen that the proposed method achieves the highest recovery rate and owns distinct advantage. While the other two methods have similar recovery rates, the Bayesian compressive sensing performs better but the gap is small. When the missing point is smaller than 75%, the recovered TFR ratio approximately achieves 60%. When the available sample ratio is larger than 40%, the recovery owns rather high accuracy. Since the center frequency of signal is 200 kHz, when the available sample ratio is 40% the equivalent sampling rate will be equal to the Nyquist rate. Under this sample ratio, the recovery ratio is larger than 70%. Therefore, this relation shown in Fig. 9 demonstrates that even when the signal is in the sub-Nyquist sampling, the compressive sensing can assist to reconstruct the time-frequency distribution. It is worth noting that although the data compression and data missing problem can be solved by compressive sensing to some degree, the post-processing is computationally expensive and also timeconsuming. This is because that the complex numeration is brought by the recovery from only few data.

.

4. Experimental verification and discussion

4.1 Experimental investigation and comparison

The Lamb wave inspection of a large plate (1.5 m x 1.5 m) is chosen for the experiment. Multiple transmitters and receivers are placed on the two sides of a metallic plate. The configuration is shown in Fig. 10. The transmitter will be excited in turn and all the receivers will receive the Lamb wave. In the center of the plate, one circle defect is built to simulate the actual damage.

The adopted numbers of transmitter and receiver are both 10. Thus, the amount of different transmitter–receiver pairs is equal to 10 x 10. The experiment waveform will subtract the baseline signal to reduce the wave from fixed boundary reflection. For transmitter #5 and receiver #5, the received waveform in the undersampled way is depicted in Fig. 11.

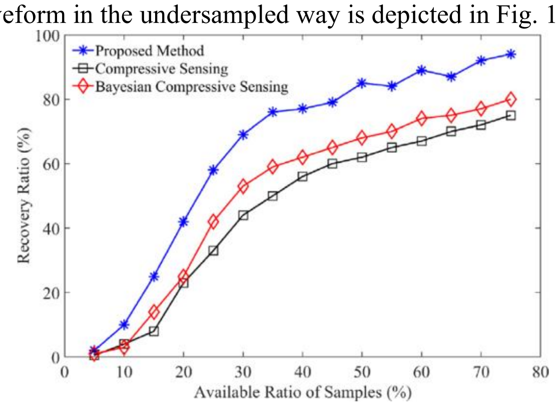

Fig.9. The recovery ratio of TFR grids under different ratios of available samples.

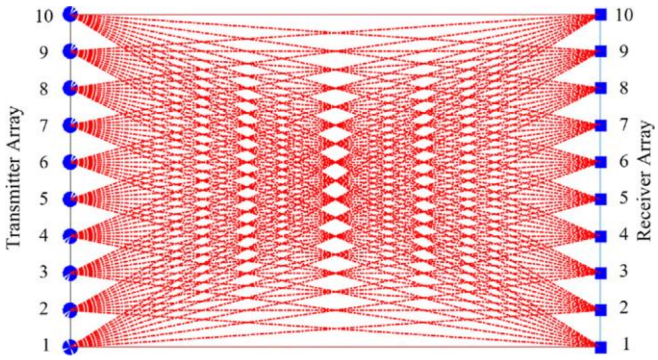

Fig. 10. The configuration of transmitter and receiver array for the plate tomography.

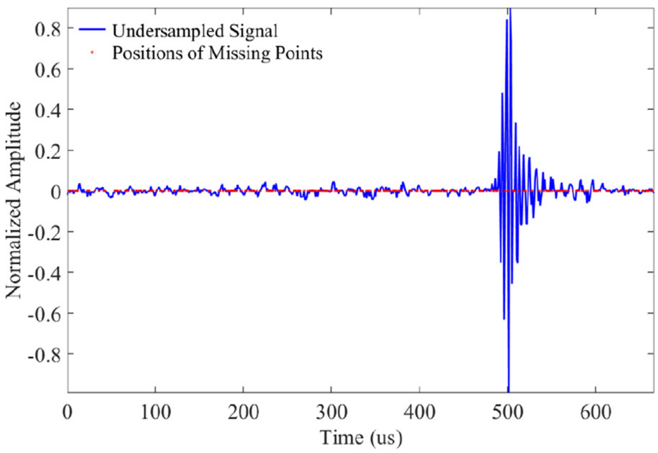

Fig.11. The undersampled wavefrom the pair of transmitter #5and receiver #5.

Similar with the simulation the original sampling rate is 1 MHz and only 60% of the original samples are available. The other samples are set as zero considering the data compression or data missing. It can be seen that the evident noise is introduced in the signal due to the experimental environment.

The reconstruction of TFR is conducted using the proposed scheme and the results are shown in Fig. 12a. It can be observed that the time-frequency distribution is recovered in an accurate way. Meanwhile, the TFR is clear and clean, nearly without interference. The noise problem is overcome by the sensing process. The result of direct TFR of the undersampled signal is shown in Fig. 12b. It can be found that with the lost information, the blurs appear in the TFR and make the components difficult to identify.

To validate the superiority of structural sparse Bayesian compressive sensing, the comparisons with conventional compressive sensing and Bayesian compressive sensing are conducted. For commonly used compressive sensing, the inverse process of the model (3) can be described as the solution for:

$$\hat{\mathbf{s}} = \text{argmin}\|\mathbf{s}\|_1 \quad \text{s.t.} \quad \mathbf{y} = \Theta\mathbf{s} \quad (24)$$

where the notation kk1 means the l1 norm term. This equation can be considered as an optimization problem and then the corresponding algorithms can be used to solve it. The orthogonal matching pursuit (OMP) is adopted in this work and the results are shown in Fig. 12c. It can be observed that the ag

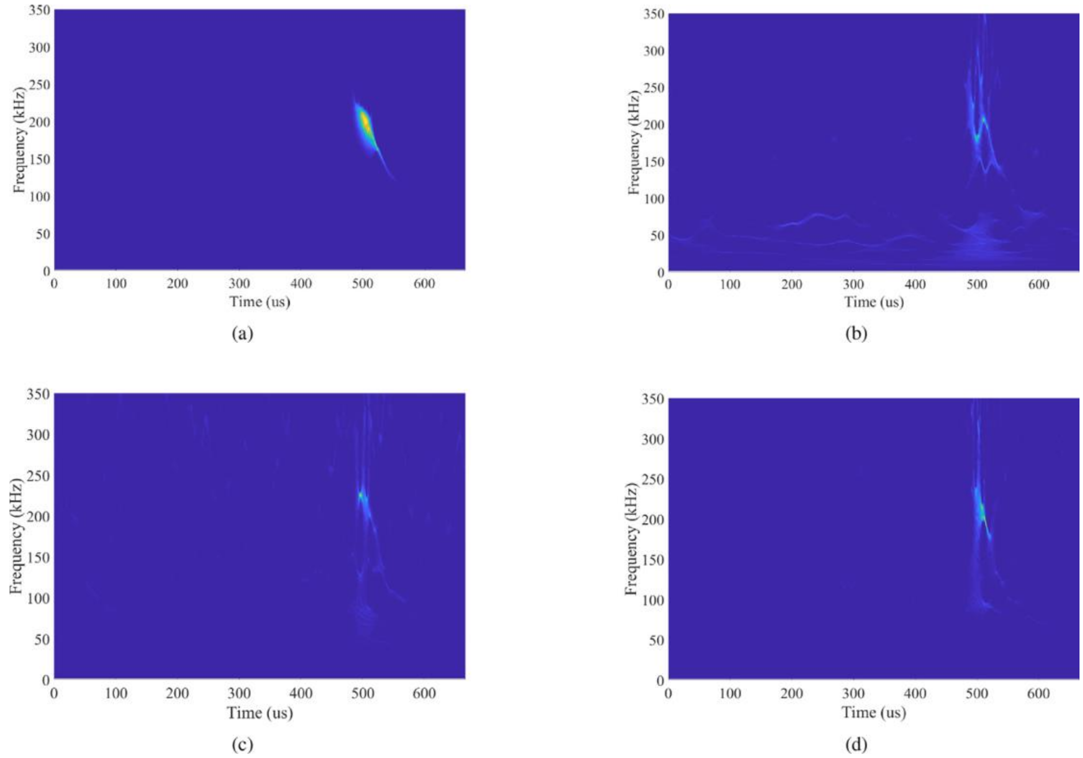

Fig.12. The TFR from proposed method and other three methods for comparison. (a) recovery ratio of TFR grids under different ratios of available samples.

gregate time-frequency distribution can be identified. However, some disturbances of time-frequency distributions appear in the arrival time of wavepacket and the contour of this area is relatively blurred.

For the conventional Bayesian compressive sensing, it only utilizes the sparse property but not the structural prior information in TFR. The results are presented in Fig. 12d. Due to the lack of the structural sparse prior, the recovered TFR is not coherent in the inner part of the concentrated distribution area. The timefrequency distribution is not as concentrated as that in the results from proposed scheme.

Furthermore, the direct TFR of original signal without undersampling is shown in Fig. 13. It can be seen that the TFR presents the aggregated feature and the usage of structural sparsity is reasonable. By comparing Fig. 13 and 12a, the TFR are recovered in most of the grids when using the proposed method.

The differential signal-to-noise ratios (SNR) are also considered to evaluate the performance of proposed method. The

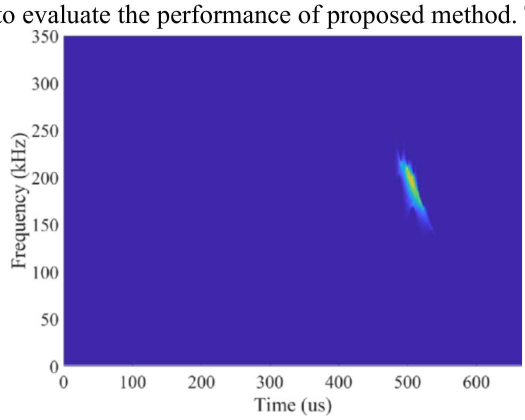

Fig. 13. The direct TFR of original signal without undersampling in the experiment.

Gaussian noise is introduced to the signal. For SNR of 5, 10, 15 and 20 dB, the recovery rates are calculated and the results are shown in Table 2. When facing the noisy environment in the Lamb wave inspection site, the proposed method can still recover the TFR. However, when the SNR is smaller than 10db, the recovery rate drops distinctly.

4.2 Further discussion

The TFR can facilitate the analysis of Lamb wave in a two-dimensional plane. In this plane, the time-relevant or frequency relevant or time-frequency characteristics can be further extracted. In this context, the maximum energy time-frequency ridge is considered. Through the ridge, the time information corresponding to the excitation frequency of Lamb wave can be obtained. The mathematical expression for the ridge is shown as follows:

$$Ri(n,f) = \underset{f}{\operatorname{argmax}}\ \mathbf{C}(\mathbf{n},\mathbf{f}); \quad \forall n \tag{25}$$

where Ri is the extracted ridge.

The time information can be further obtained from the energy ridge readily. Then the TOF can be used in damage localization or tomography. By using (25), the energy ridge and TOF can be extracted. To demonstrate the effectiveness of TOF extraction, multiple TOFs are compared with the theoretical values from the ray tracing (RT) technique. The value from RT can be regarded as the true TOF. We also conducted the TOF calculation from commonly used threshold method and cross correlation method. In the threshold method, the signal amplitude of 10% of maximum amplitude is used to measure the arrival of the wavepacket. In the cross correlation method, the correlation of received signal and excitation signal is employed to obtain the TOF. Fig. 14 presents the results from all the receivers with the transmitter #1 at work. It

Table 2
The recovery rates under differential signal-to-noise ratios.

Signal-to-noise ratio	5	10	15	20
Recovery rate	41.6	59.5	67.1	72.3

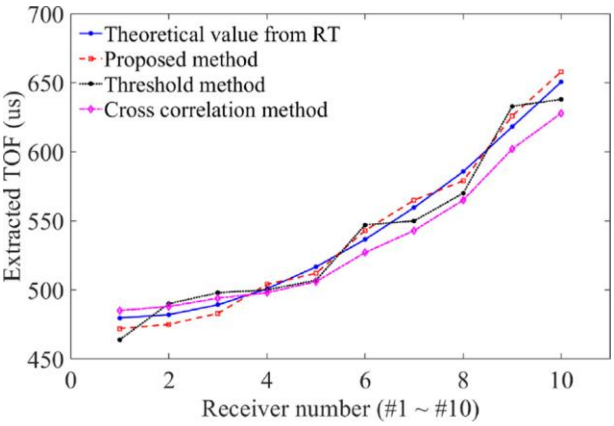

Fig. 14. The theoretical TOF from the ray tracing and the obtained TOF from other three methods. The waveforms from receivers (#1 ~#10) is adopted

can be seen that the proposed method presents robust and accurate TOF extraction capacity. While for the threshold method, the values experience drastic fluctuate with different propagation routes. The errors brought by the cross correlation method become distinct when the waves propagate longer distances. The relative errors are numerically calculated and they are no larger than 3% for the proposed method. When more samples are available, the relative error of TOF can be further decreased.

The TOF is the input for the Lamb wave tomography. The slight disturbance in TOF might cause apparent differences due to the inherent characteristic of its iterative algorithm. Therefore, the accurate TOF is vital. After extracting all the TOFs, the tomography using the simultaneous iterative reconstruction technique is implemented and the obtained image is shown in Fig. 15. It can be seen that the damage region forms larger values than the surrounding medium. However, the imaging is not elaborate since the transducer number is not large enough. When more transducers are applied, the data compression problem will become more important.

For the TFR from the conventional compressed sensing and Bayesian compressive sensing, when extracting the maximum energy ridge, the TFR values with deficient concentration bring interference and the ridge can not be successfully

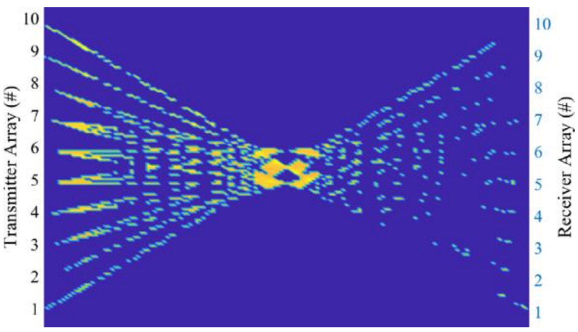

Fig.9. The results of Lamb wave tomography using the TOF as the input data..

extracted in some discrete time points. The obtained TOF also presents a larger error in the array signal processing. Therefore, the proposed method combining the sparse prior in two-dimensional plane outperforms the conventional Bayesian compressive sensing which considers the recovery in a one-dimensional situation. Meanwhile, the advantage also follows with the price of longer computation time.

5. Conclusion and future directions

In this paper, a new scheme for time-frequency distribution recovery directly from the undersampled signal is proposed. The conventional Bayesian compressive sensing is modified through utilizing the structural sparse prior in the TFR of disperse Lamb wave signal. In the investigation using the simulated signal, the TFR is accurately reconstructed. The recovery from different subsampling cases indicates that when the available sample ratio is larger than 25%, the recovery rate of TFR is satisfactory. Even when the equivalent sampling rate is under the Nyquist rate, the TFR can be reconstructed to some extent. In the experimental validation, signals from different transmitter–receiver pairs are adopted to implement the proposed method. The relative error of TOF characteristic extracted from the TFR is smaller than 3%. Compared with current methods, the designed scheme is superior than conventional compressive sensing. However, it also brings a higher computation complexity. In the future, the damage imaging directly recovered from the compressed signal is promising in the situation where there is high demand for visualization.

References

[1] Senyurek VY. Detection of cuts and impact damage at the aircraft wing slat by using Lamb wave method. Measurement 2015;67:10–23.
[2] Masurkar FA, Yelve NP. Optimizing location of damage within an enclosed area defined by an algorithm based on the lamb wave response data. Appl Acoust 2017;120:98–110.
[3] Yelve NP, Mitra M, Mujumdar PM. Detection of delamination in composite laminates using Lamb wave based nonlinear method. Compos Struct 2017;159:257–66.
[4] Wang Z, Huang S, Wang S, Wang Q, Zhao W. Multifrequency identification and exploitation in Lamb wave inspection. IEEE Access 2019;7. pp. 150 435– 150 443.
[5] Zhang B, Hong X, Liu Y. Multi-task deep transfer learning method for guided wave-based integrated health monitoring using piezoelectric transducers. IEEE Sens J 2020;20(23). pp. 14 391–14 400.
[6] De Marchi L, Perelli A, Marzani A. A signal processing approach to exploit chirp excitation in Lamb wave defect detection and localization procedures. Mech Syst Signal Process 2013;39(1–2):20–31.
[7] Huthwaite P, Simonetti F. High-resolution guided wave tomography. Wave Motion 2013;50(5):979–93.
[8] Zhang J, Ma H, Yan W, Li Z. Defect detection and location in switch rails by acoustic emission and lamb wave analysis: a feasibility study. Appl Acoust 2016;105:67–74.
[9] Su C, Jiang M, Liang J, Tian A, Sun L, Zhang L, Zhang F, Sui Q, et al. Damage identification in composites based on hilbert energy spectrum and lamb wave tomography algorithm. IEEE Sens J 2019;19(23). pp. 11 562–11 572.
[10] Hu Y, Zhu Y, Tu X, Lu J, Li F. Dispersion curve analysis method for Lamb wave mode separation. Struct Health Monitor 2019. p.

147592171989059.
[11] Fateri S, Boulgouris NV, Wilkinson A, Balachandran W, Gan T. Frequencysweep examination for wave mode identification in multimodal ultrasonic guided wave signal. IEEE Trans Ultrason Ferroelectr Freq Control 2014;61 (9):1515–24.
[12] Wang S, Huang S, Wang Q, Zhang Y, Zhao W. Mode identification of broadband lamb wave signal with squeezed wavelet transform. Appl Acoust 2017;125:91–101.
[13] Mitra M, Gopalakrishnan S. Guided wave based structural health monitoring: a review. Smart Mater Struct 2016;25(5):53001.
[14] Fathi H, Kazemirad S, Nasir V. Lamb wave propagation method for nondestructive characterization of the elastic properties of wood. Appl Acoust 2021;171:107565.
[15] Wang Z, Huang S, Wang S, Wang Q, Zhao W. A damage localization method with multimodal lamb wave based on adaptive polynomial chirplet transform. IEEE Trans Instrum Meas 2020;69(10):8076–87.
[16] Yu L, Tian Z, Leckey CAC. Crack imaging and quantification in aluminum plates with guided wave wavenumber analysis methods. Ultrasonics 2015;62:203–12.
[17] Zhou K, Zheng Y, Zhang J, Xu X, Ma S, Wu Z. A reconstruction-based mode separation method of lamb wave for damage detection in plate structures. Smart Mater Struct 2019;28(3). p. 035033.
[18] Wang P, Zhou W, Li H. A singular value decomposition-based guided wave array signal processing approach for weak signals with low signal-to-noise ratios. Mech Syst Signal Process 2020;141. p. 106450.
[19] Zoubi AB, Kim S, Adams DO, Mathews VJ. Lamb wave mode decomposition based on Cross-Wigner-Ville distribution and its application to anomaly imaging for structural health monitoring. IEEE Trans Ultrason Ferroelectr Freq Control 2019;66(5):984–97.
[20] Hosseinabadi HZ, Nazari B, Amirfattahi R, Mirdamadi HR, Sadri AR. Wavelet network approach for structural damage identification using guided ultrasonic waves. IEEE Trans Instrum Meas 2014;63(7):1680–92.
[21] De Marchi L, Marzani A, Caporale S, Speciale N. Ultrasonic guided-waves characterization with warped frequency transforms. IEEE Trans Ultrason Ferroelectrics Frequency Control 2009;56(10):2232–40.
[22] Benammar A, Drai R, Guessoum A. Ultrasonic flaw detection using threshold modified S-transform. Ultrasonics 2014;54(2):676–83.
[23] Kim C-Y, Park K-J. Mode separation and characterization of torsional guided wave signals reflected from defects using chirplet transform. NDT & E Int 2015;74:15–23.
[24] Zeng L, Zhao M, Lin J, Wu W. Waveform separation and image fusion for lamb waves inspection resolution improvement. NDT & E Int 2016;79(Supplement C):17–29.
[25] Ji S, Tan C, Yang P, Sun Y-J, Fu D, Wang J. Compressive sampling and data fusion-based structural damage monitoring in wireless sensor network. J Supercomput 2018;74(3):1108–31.
[26] Perelli A, Ianni T, Marzani A, Marchi L, Masetti G. Model-based compressive sensing for damage localization in lamb wave inspection. IEEE Trans Ultrason, Ferroelectrics Frequency Control 2013;60(10):2089–97.
[27] Wang Z, Huang S, Wang S, Zhuang S, Wang Q, Zhao W. Compressed sensing method for health monitoring of pipelines based on guided wave inspection IEEE Trans Instrum Meas 2020;69(7):4722–31.
[28] Xu C-B, Yang Z-B, Chen X-F, Tian S-H, Xie Y. A guided wave dispersioncompensation method based on compressed sensing. Mech Syst Signal Process 2018;103:89–104.
[29] Zhang S, Zhang YD. Robust time-frequency analysis of multiple fm signals with burst missing samples. IEEE Signal Process Lett 2019;26(8):1172–6.
[30] Wang Z, Huang S, Wang S, Wang Q, Zhao W. Sparse reconstruction based timefrequency representation for time-of-flight extraction of undersampled Lamb wave signal. In: Proc. Conf. Precis. Electrom. Meas. (CPEM); Aug. 2020. p. 1–2..
[31] Jayawardhana M, Zhu X, Liyanapathirana R, Gunawardana U. Compressive sensing for efficient health monitoring and effective damage detection of structures. Mech Syst Signal Process 2017;84:414–30.
[32] Wang W, Bao Y, Zhou W, Li H. Sparse representation for wanghuang-1381- wave-based damage detection using a dictionary algorithm. Ultrasonics 2018;87:48–58.
[33] Ji S, Xue Y, Carin L. Bayesian compressive sensing. IEEE Trans Signal Process 2008;56(6):2346–56.
[34] Yu L, Sun H, Barbot JP, Zheng G. Bayesian compressive sensing for cluster structured sparse signals. Signal Process 2012;92(1):259–69.
[35] Donoho DL. Compressed sensing. IEEE Trans Inform Theory 2006;52 (4):1289–306.
[36] Jokanovic B, Amin M. Reduced interference sparse time-frequency distributions for compressed observations. IEEE Trans Signal Process2015;63(24):6698–709.
[37] Fang J, Shen Y, Li H, Wang P. Pattern-coupled sparse bayesian learning for recovery of block-sparse signals. IEEE Trans Signal Process 2015;63(2):360–72.
[38] Rangan S. Generalized approximate message passing for estimation with random linear mixing. IEEE International Symposium on Information Theory Proceedings 2011;2011:2168–72.
[39] Fang J, Zhang L, Li H. Two-dimensional pattern-coupled sparse bayesian learning via generalized approximate message passing. IEEE Trans Image Process 2016;25(6):2920–30.